SLAC-PUB-12887

Hyperon And Hyperon Resonance Properties From Charm Baryon Decays At *BABAR*

Veronique Ziegler

Department of Physics and Astronomy, The University of Iowa, Iowa City, IA 52242, USA

E-mail: vziegler@slac.stanford.edu

Abstract. We present studies of hyperon and hyperon resonance production in charm baryon decays at *BABAR*. Using two-body decays of the Ξ_c^0 and Ω_c^0, we are able to show, for the first time, that the spin of the Ω^- is 3/2. The analysis procedures are extended to three-body final states and properties of the $\Xi(1690)^0$ are extracted from a detailed isobar model analysis of the $\Lambda_c^+ \to \Lambda K_S K^+$ Dalitz plot. Similar techniques are then used to study $\Xi(1530)^0$ production in Λ_c^+ decay.

1. Introduction

The data samples used for the analyses described in this note were collected with the *BABAR* detector at the PEP-II asymmetric-energy e^+e^- collider. In these studies the charm baryons are inclusively produced in e^+e^- collisions at center-of-mass energies 10.58 and 10.54 GeV. The *BABAR* detector and reconstruction software are described elsewhere [1].

2. General Procedure for Charm Baryon Selection

The selection of charm baryon candidates requires the sequential reconstruction of initial and intermediate state candidates using four-momentum addition of tracks. Particle identification selectors based on specific energy loss ($\mathrm{d}E/\mathrm{d}x$) and Cherenkov angle measurements have been used to identify proton, pion and kaon final tracks. Each intermediate state candidate is required to have its invariant mass within $\pm 3\sigma$ of the fitted peak position of the relevant distribution, where σ is the mass resolution. In all cases, the fitted peak mass is consistent with the expected value, and the intermediate state invariant mass is then constrained to this value. Due to the fact that each weakly-decaying intermediate state (i.e. the K_S and hyperons) is long-lived, the signal-to-background ratio is improved by imposing a vertex displacement criterion (in the direction of the momentum vector). In order to further enhance signal-to-background ratio, a selection criterion is imposed on the center-of-mass momentum p^* of the parent charm baryon. The use of charge conjugate states is implied throughout in this note.

3. Measurement of the Spin of the Ω^-

The $SU(3)$ classification scheme predicted [2] the existence of the Ω^- hyperon, an isosinglet with hypercharge $Y = -2$ and strangeness $S = -3$, as a member of the $J^P = 3/2^+$ ground state baryon decuplet. Such a particle was observed subsequently with the predicted mass in a bubble chamber experiment [3]. In previous attempts to confirm the spin of the Ω^- [4, 5, 6],

Contributed to 2nd Meeting of the APS Topical Group on Hadronic Physics, 10/22/2006--10/24/2006, Nashville, Tennesse

Work supported in part by US Department of Energy contract DE-AC02-76SF00515

SLAC, Stanford University, Stanford, CA 94025

K^- p interactions in a liquid hydrogen bubble chamber were studied. In each case only a small Ω^- data sample was obtained, and the Ω^- production mechanism was not well understood. As a result, these experiments succeeded only in establishing that the Ω^- spin is greater than 1/2.

In this study [7], measurements of the Ω^- spin are obtained using a primary sample obtained from the decay sequence $\Xi_c^0 \to \Omega^- K^+$, with $\Omega^- \to \Lambda K^-$, while a much smaller sample resulting from $\Omega_c^0 \to \Omega^- \pi^+$, with $\Omega^- \to \Lambda K^-$ is used for corroboration. In each case the Λ is reconstructed in the decay mode $\Lambda \to p\pi^-$. It is assumed that each charm baryon type has spin 1/2 and, as a result of its inclusive production, that it is described by a diagonal spin projection density matrix. The analysis does not require that the diagonal matrix elements be equal.

By choosing the quantization axis along the direction of the Ω^- in the charm baryon rest-frame, the Ω^- inherits the spin projection of the charm baryon [7]. It follows that, regardless of the spin J of the Ω^-, the density matrix describing the Ω^- sample is diagonal, with non-zero values only for the $\pm 1/2$ spin projection elements, i.e. the helicity λ_i of the Ω^- can take only the values $\pm 1/2$. Since the final state Λ and K^- have spin values 1/2 and 0, respectively, the net final state helicity λ_f also can take only the values $\pm 1/2$.

Defining the helicity angle θ_h as the angle between the direction of the Λ in the rest-frame of the Ω^- and the quantization axis, the probability for the Λ to be produced with Euler angles $(\phi, \theta_h, 0)$ with respect to the quantization axis is given by the square of the amplitude ψ, characterizing the decay of an Ω^- with spin J and helicity λ_i to a 2-body system with net helicity λ_f, where $\psi = A^J_{\lambda_f} D^{J\,*}_{\lambda_i \lambda_f}(\phi, \theta_h, 0)$, and the transition matrix element $A^J_{\lambda_f}$ represents the coupling of the Ω^- to the final state. The angular distribution of the Λ is then given by

$$I \propto \sum_{\lambda_i, \lambda_f} \rho_{i\,i} \left| A^J_{\lambda_f} D^{J\,*}_{\lambda_i \lambda_f}(\phi, \theta_h, 0) \right|^2 , \tag{1}$$

where the $\rho_{i\,i}$ ($i = \pm 1/2$) are the diagonal density matrix elements inherited from the charm baryon, and the sum is over all initial and final helicity states. The Λ angular distribution integrated over ϕ is then obtained for spin hypotheses $J_\Omega = 1/2$, 3/2, and 5/2, respectively as follows:

$$dN/d\cos\theta_h \propto 1 + \beta \cos\theta_h \tag{2}$$

$$dN/d\cos\theta_h \propto 1 + 3\cos^2\theta_h + \beta \cos\theta_h (5 - 9\cos^2\theta_h) \tag{3}$$

$$dN/d\cos\theta_h \propto 1 - 2\cos^2\theta_h + 5\cos^4\theta_h + \beta \cos\theta_{\rm h} (5 - 26\cos^2\theta_h + 25\cos^4\theta_h), \tag{4}$$

where the coefficient of the asymmetric term, β [7], may be non-zero as a consequence of parity violation in charm baryon and Ω^- weak decay.

The efficiency-corrected $\cos\theta_h(\Lambda)$ distribution with fits corresponding to Eq. (3) with $\beta \neq 0$ and $\beta = 0$ is shown in Fig. 1 (a); Fig. 1 (b) shows the same distribution with fits corresponding to Eqs. (2) and (4) with $\beta = 0$. The fit results are summarized in Table 1, and clearly $J = 3/2$ is strongly preferred.

These results were checked using the sample of Ω^- hyperons obtained from Ω_c baryon decays and very good agreement was obtained.

We remark that for $J_{\Xi_c} = 3/2$, $J_\Omega = 5/2$ is entirely acceptable; the determination of the Ω^- spin is contingent upon the generally-accepted assumption that the spin of the Ξ_c^0 (and Ω_c^0) is 1/2.

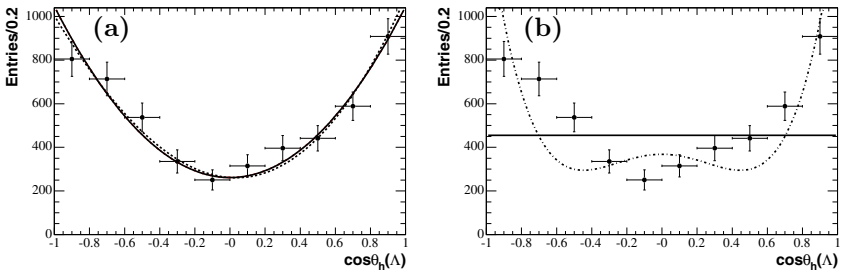

Figure 1. (a) The efficiency-corrected $\cos\theta_h(\Lambda)$ distribution for $\Xi_c^0 \to \Omega^- K^+$ data. The dashed curve shows the $J_\Omega = 3/2$ fit using Eq. (3), in which β allows for possible asymmetry. This fit yields $\beta = 0.04 \pm 0.06$. The solid curve represents the corresponding fit with $\beta = 0$. (b) For the same data and $\beta = 0$, the solid line represents the expected distribution for $J_\Omega = 1/2$, while the dashed curve corresponds to $J_\Omega = 5/2$. The fit results are given in Table 1.

J_Ω	Fit χ^2/NDF	Fit C.L.	Comment
1/2	100.4/9	1×10^{-17}	Fig. 1 (b), solid line
3/2	6.5/9	0.69 ($\beta = 0$)	Fig. 1 (a), solid curve
3/2	6.1/8	0.64 ($\beta \neq 0$)	Fig. 1 (a), dashed curve
5/2	47.6/9	3×10^{-7}	Fig. 1 (b), dashed curve

Table 1. The $\cos\theta_h(\Lambda)$ angular distribution fit C.L. values corresponding to Ω^- spin hypotheses 1/2, 3/2 and 5/2 for $\Xi_c^0 \to \Omega^- K^+$ data assuming $J_{\Xi_c} = 1/2$. For $J_\Omega \geq 7/2$, the predicted angular distribution increases even more steeply for $|\cos\theta_{\rm h}| \sim 1$ than for $J_\Omega = 5/2$, and can be excluded at C.L. greater than 99%.

3.1. The Use of Legendre Polynomial Moments in Spin Determination

For Ω^- spin J, the corrected angular distributions can be written

$$\frac{dN}{d\cos\theta_h} = N \left[\sum_{l=0}^{l_{max}} \langle P_l \rangle P_l \left(\cos\theta_h \right) \right],$$

where $P_l\left(\cos\theta_h\right)$ are normalized Legendre Polynomial functions such that $l_{max} = 2J - 1$, and if l is odd $\langle P_l \rangle = 0$. Each assumed J defines l_{max}, so that $\langle P_l \rangle = 0$ for $l > l_{max}$ and $\langle P_l \rangle$ is calculable. The number of Ω^- signal events in a given mass bin is obtained by giving each event, j, in that bin, a weight $w_j = \frac{P_{l_{max}}\left(\cos\theta_{h_j}\right)}{\langle P_{l_{max}} \rangle}$.

In particular, for $J = 3/2$, giving each event a weight $w_j = \sqrt{10} P_2(\cos\theta_{h_j})$ projects the complete Ω^- signal. In order to test the $J = 5/2$ hypothesis, each event is given a weight $w_j = \frac{7}{\sqrt{2}} P_4(\cos\theta_{h_j})$. Figure 2 shows the Ω^- invariant mass distribution corresponding to the $\Xi_c^0 \to \Omega^- K^+$ mass-signal region ($2.452 < m < 2.488$ GeV/c^2). The solid histogram represents the efficiency-corrected, unweighted Ω^- mass spectrum, while the open circles represent the efficiency-corrected (a) $\sqrt{10} P_2(\cos\theta_h)$ and (b) $7/\sqrt{2} P_4(\cos\theta_h)$ moments of the distribution. As expected, the $\sqrt{10} P_2(\cos\theta_h)$ moment projects out the Ω^- signal, whereas the $7/\sqrt{2} P_4(\cos\theta_h)$ moment does not.

4. Study of Cascade Resonances Using Three-body Charm Baryon Decays

Although considerable advances have been made in baryon spectroscopy over the past decade, there has been very little improvement in our knowledge of hyperon resonances since 1988. The

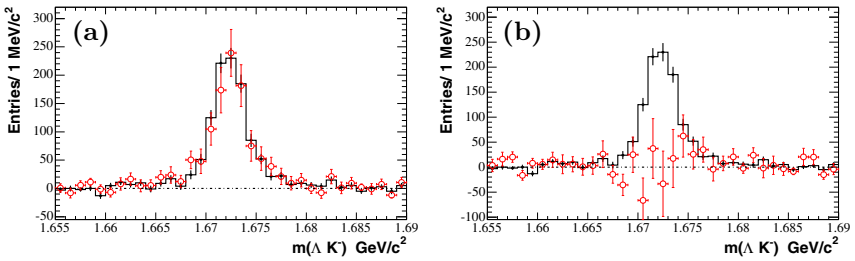

Figure 2. The efficiency-corrected normalized (a) $\sqrt{10}P_2(\cos\theta(\Lambda))$ and (b) $7/\sqrt{2}P_4(\cos\theta(\Lambda))$-weighted distributions (open circles) as a function of Ω^- invariant mass obtained from $\Xi_c^0 \to \Omega^- K^+$ events; the solid histogram shows the corrected Ω^- mass spectrum for the Ξ_c^0 mass-signal region.

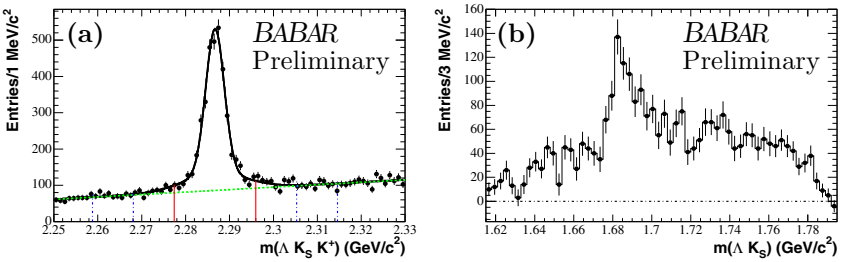

Figure 3. (a) The invariant mass distribution of uncorrected $\Lambda K_S K^+$ candidates in ~ 200 fb^{-1} of data. The superimposed curve corresponds to a binned χ^2 fit which uses a double Gaussian signal function and a linear background parametrization. A signal yield of 2900 ± 105 candidates is obtained from this fit. The vertical lines delimit the signal region used in this analysis (solid) and the corresponding mass-sideband regions (dotted) used to study the background contribution in the signal region. (b) The Λ_c^+ mass-sideband-subtracted ΛK_S invariant mass projection of uncorrected $\Lambda K_S K^+$ candidates in ~ 200 fb^{-1} of data.

$\Xi(1690)$ has been observed in the $\Lambda\bar{K}$, $\Sigma\bar{K}$ and $\Xi\pi$ final states with various degrees of certainty. Its quantum numbers have not yet been measured. The $\Xi(1530)$ has primarily been seen via its decay to $\Xi^-\pi^+$, however its spin-parity remains uncertain.

4.1. The $\Xi(1690)^0$ from $\Lambda_c^+ \to (\Lambda\bar{K}^0)K^+$ Decay

The $\Xi(1690)^0$ is observed in the $\Lambda\bar{K}^0$ system produced in the decay $\Lambda_c^+ \to (\Lambda\bar{K}^0)K^+$, where the $\bar{K}^0$ is reconstructed via $K_S \to \pi^+\pi^-$. The data sample analyzed corresponds to a total integrated luminosity of about 200 fb^{-1} [8].

The selection of Λ_c^+ candidates requires the intermediate reconstruction of oppositely-charged track pairs consistent with $\Lambda \to p\,\pi^-$ and $K_S \to \pi^+\,\pi^-$ decays. The invariant mass spectrum of the resulting Λ_c^+ candidates before efficiency-correction and the $\Lambda\bar{K}^0$ mass distribution corresponding to the Λ_c^+ signal region are shown in Fig. 3 (a) and (b), respectively. A clear peak is seen in the vicinity of the $\Xi(1690)^0$; it should be noted that this signal is skewed significantly toward high mass.

The second and fourth order Legendre polynomial moments as a function of the mass of the (ΛK_S) system display no peaking structure at the position of the $\Xi(1690)^0$, which suggests that the $\Xi(1690)^0$ spin is probably 1/2. However, the Λ helicity cosine ($\cos\theta_\Lambda$) distribution is not flat in contrast to the expectation for a spin 1/2 to 1/2 transition. The Dalitz plot of $\Lambda_c^+ \to \Lambda\bar{K}^0 K^+$

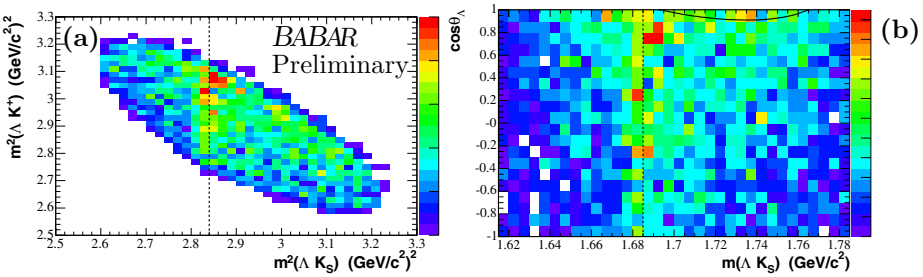

Figure 4. (a) The Dalitz plot for $\Lambda_c^+ \to \Lambda \bar{K}^0 K^+$ corresponding to the Λ_c^+ signal region indicated in Fig. 3. The dashed line indicates the nominal mass-squared region of the $\Xi(1690)^0$. (b) The rectangular Dalitz plot for $\Lambda_c^+ \to \Lambda \bar{K}^0 K^+$ corresponding to the Λ_c^+ signal region indicated in Fig. 3. The black curve corresponds to the $a_0(980)^+$ pole position.

signal candidates is shown, without efficiency-correction, in Fig. 4 (a). A clear band is observed in the mass-squared region of the $\Xi(1690)^0$, together with an accumulation of events in the $\bar{K}^0 K^+$ threshold region; the latter is consistent with a contribution to the Dalitz plot due to the $a_0(980)^+$ resonance. In contrast, the Dalitz plots corresponding to the Λ_c^+ mass-sideband regions exhibit no structure.

We attempt to describe the event distribution in the Dalitz plot of Fig. 4 (b) in terms of an isobar model consisting of the coherent superposition of amplitudes characterizing $(\Lambda a_0(980)^+)$ and $(\Xi(1690)^0 K^+)$ decay of the Λ_c^+. The $a_0(980)$ is known to couple to both $\eta\pi$ and $\bar{K}K$ and is characterized by the Flatté parametrization [9], while a Breit-Wigner function is used to describe the amplitude for the $\Xi(1690)^0$.

This model is used to describe the intensity distribution at a point on the Dalitz plot by means of the squared modulus of a coherent superposition of these two amplitudes, under the assumption that the $\Xi(1690)^0$ has spin 1/2, since the moment projections favor this choice. Fits to the Dalitz plot under the assumptions of spin 3/2 and 5/2 are ongoing. We find that no additional isobars are needed in order to accurately model the data. In order to extract the mass and width parameters of the $\Xi(1690)^0$, we perform a binned maximum Likelihood fit to the rectangular plot of Fig. 4 (b), incorporating resolution smearing in mass, and a background parametrization obtained from the Λ_c^+ mass-sidebands.

The fit reproduces accurately the skewed lineshape of the ΛK_S invariant mass projection. The skewing results from the interference between the $a_0(980)^+$ and the $\Xi(1690)^0$. The actual $\Xi(1690)^0$ signal is symmetric and significantly smaller than the apparent signal, which is dominated by this interference effect. The fit also provides an excellent representation of the other invariant mass projections. Final results on the mass and width parameter values for the $\Xi(1530)^0$ are in preparation.

4.2. The Properties of the $\Xi(1530)^0$ *from* $\Lambda_c^+ \to \Xi^-\pi^+K^+$ *Decay*

The Dalitz plot for $\Lambda_c^+ \to \Xi^-\pi^+K^+$ is dominated by the contribution from $\Lambda_c^+ \to \Xi(1530)^0 K^+$, where $\Xi(1530)^0 \to \Xi^-\pi^+$ by strong decay. The projection of the $\Xi^-\pi^+$ invariant mass for the Λ_c^+ signal region of Fig. 5 (a) is shown in Fig. 5 (b). The Dalitz plot (Fig. 6) shows evidence for only one resonant structure. A clear band can be seen at the nominal mass squared of the $\Xi(1530)^0 \to \Xi^-\pi^+$.

As before, spin information for the $\Xi(1530)$ is obtained using Legendre polynomial moments. The $\sqrt{10}P_2(\cos\theta_{\Xi^-})$ moment of the $(\Xi^-\pi^+)$ system invariant mass distribution for the Λ_c^+ signal region indicates that spin 3/2 is clearly favored. On the other hand the $7/\sqrt{2}P_4(\cos\theta_{\Xi^-})$ moment is consistent with being flat implying that spin 5/2 is ruled out. These results are corroborated

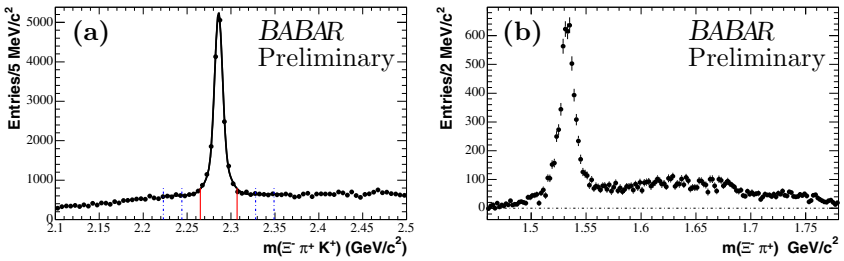

Figure 5. (a) The invariant mass distribution of uncorrected $\Xi^-\pi^+K^+$ candidates in ~ 230 fb^{-1} of data. The superimposed curve corresponds to a binned χ^2 fit which uses a double Gaussian signal function and a linear background parametrization. A signal yield of ~ 13800 candidates is obtained from this fit. The vertical lines delimit the signal region used in this analysis (solid) and the corresponding mass-sideband regions (dotted). (b) The Λ_c^+ mass-sideband-subtracted $\Xi^-\pi^+$ invariant mass projection of uncorrected $\Xi^-\pi^+K^+$ candidates in ~ 230 fb^{-1} of data.

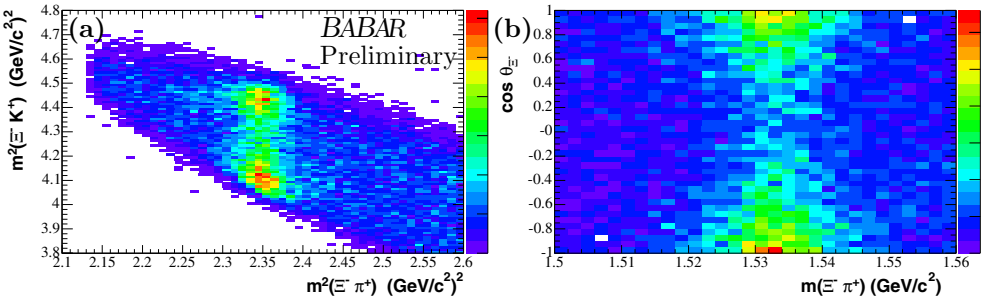

Figure 6. (a) The Dalitz plot of the Ξ^-K^+ versus the $\Xi^-\pi^+$ invariant mass-squared distribution corresponding to the Λ_c^+ signal region. (b) The corresponding rectangular Dalitz plot for the $\Xi(1530)^0$ mass region.

by the $\alpha\,(1+3\cos^2\theta)$ behavior of the $\cos\theta_{\Xi^-}$ distribution corresponding to the $\Xi(1530)^0$ signal region. Schlein *et al.* [10] showed that $J^P = 3/2^+$ or $J^P = 5/2^-$ and claimed $J > 3/2$ not required, thereby concluding that $J^P = 3/2^+$ was favored by their data. Therefore, the present analysis by establishing $J = 3/2$ also establishes positive parity by implication. An amplitude analysis of the $\Xi^-\pi^+$ system in terms of a model incorporating S, P and D waves is currently in progress.

5. Conclusions

The angular distributions of the decay products of the Ω^- baryon resulting from Ξ_c^0 and Ω_c^0 decays are well-described by a function $\propto (1+3\cos^2\theta_h)$. These observations are consistent with spin assignments 1/2 for the Ξ_c^0 and the Ω_c^0, and 3/2 for the Ω^-. Values of 1/2 and greater than 3/2 for the spin of the Ω^- yield C.L. values significantly less than 1% when spin 1/2 is assumed for the parent charm baryon.

Mass and width measurements for the $\Xi(1690)^0$ have been obtained from fits to the $\Lambda_c^+ \to \Lambda K_S K^+$ Dalitz plot. Preliminary results indicate that the spin of the $\Xi(1690)$ is consistent with 1/2. Tests of higher spin hypotheses are in progress.

The properties of the $\Xi(1530)^0$ are studied using the decay $\Lambda_c^+ \to \Xi^-\pi^+K^+$. The spin of the $\Xi(1530)$ is consistent with 3/2. An amplitude decomposition of the entire $\Xi^-\pi^+$ mass

distribution will be undertaken in the near future.

Acknowledgments
This work is supported by the Department of Energy (US).

References
[1] B. Aubert *et al.*, Nucl. Instr. Meth. **A479**, 1 (2002).
[2] M. Gell-Mann, Proceedings of the International Conference on High-Energy Physics, p. 805 (1962).
[3] V. E. Barnes *et al.*, Phys. Rev. Lett. **12**, 204 (1964).
[4] M. Deutschmann *et al.*, Phys. Lett. **B73**, 96 (1978).
[5] M. Baubillier *et al.*, Phys. Lett. **B78**, 342 (1978).
[6] R. J. Hemingway, *et al.*, Nucl. Phys. **B142**, 205 (1978).
[7] B. Aubert *et al.*, Phys. Rev. Lett. **97**, 112002 (2006).
[8] B. Aubert *et al.*, hep-ex/0607043, Contributed Paper to ICHEP2006, Moscow, Russia.
[9] S. M. Flatté, Phys. Lett. **B63**, 224 (1976).
[10] P. E. Schlein *et al.*, Phys. Rev. Lett. **11**, 167 (1963); J. Button-Schafer *et al.*, Phys. Rev. **B142**, 883 (1966).